BULLETIN OF THE POLISH ACADEMY OF SCIENCES
TECHNICAL SCIENCES, Vol. 64, No. 2, 2016
DOI: 10.1515/bpasts-2016-0045

Towards development of a prototype high-temperature latent heat storage unit as an element of a RES-based energy system (part 2)

J. KARWACKI*[1], K. BOGUCKA-BYKUĆ[1], W. WŁOSIŃSKI[2], and S. BYKUĆ[3]

[1] Department of Heat Transfer, The Szewalski Institute of Fluid-Flow Machinery Polish Academy of Sciences (IMP PAN), Fiszera 14 St. Gdańsk 80-231, Poland

[2] Polish Academy of Sciences, 1 Defilad Sq., 00-901 Warszawa, Poland

[3] Department of Distributed Energy, The Szewalski Institute of Fluid-Flow Machinery Polish Academy of Sciences (IMP PAN), Fiszera 14 st. Gdańsk 80-231, Poland

Abstract. This paper presents an experimental study performed with the general aim of defining procedures for calculation and optimization of shell-and-tube latent thermal energy storage unit with metals or metal alloys as PCMs. The experimental study is focused on receiving the exact information about heat transfer between heat transfer fluid (HTF) and phase change material (PCM) during energy accumulation process. Therefore, simple geometry of heat transfer area was selected. Two configurations of shell-and-tube thermal energy storage (TES) units were investigated. The paper also highlights the emerging trend (reflected in the literature) with respect to the investigation of metal PCM-based heat storage units in recent years and shortly presents unique properties and application features of this relatively new class of PCMs.

Key words: latent heat storage (LHS), phase change material (PCM), metal alloy, middle melting point metal PCM.

Nomenclature

c – specific heat [J/kgK]
h_{SL} – latent heat [J/kg]
k – overall heat transfer coefficient [W/m^{2}K]
$\dot{m}$ – average mass flow rate [kg/s]
$\dot{q}$ – heat flux [W/m^2]
$\dot{Q}$ – heat flow rate [W]
$\dot{Q}_A$ – heat flow rate lost to environment [W]
t – temperature [°C]
Δt_{Hi} – average inlet temperature gradient [K/s]
Δt_{SL} – nominal temperature range of phase transition, Eq. (12) [K]
α – heat transfer coefficient [W/m^{2}K]
δ – material thickness [m]
λ – thermal conductivity [W/m·K]
τ – time [s]
CFD – computational fluid dynamics
DSG-CSP – direct steam generation concentrated solar power
DSC – differential scanning calorimetry
HTF – heat transfer fluid
LHS – latent heat storage
PCM – phase change material
PI – proportional-integral controller
TES – thermal energy storage

Subscripts:

A – ambient air
e – outlet value
H – heat transfer fluid (HTF)
i – inlet value
P – phase change material (PCM)
R – inner tube
SL – at phase change
Z – outer tube

1. Introduction

Phase change material (PCM) investigation is one of the two elementary stages of the development of a latent heat storage (LHS) unit, next to designing the heat exchanger. Moreover, thermo-physical properties of a PCM selected for a given working temperature of a system determine the design of the heat exchanger, and thus the whole concept of the LHS unit. Since the majority of PCMs exhibit a low thermal conductivity, the means for improving overall heat transfer in LHS systems are key research topics in this field since decades [1–9], both from material side and from heat exchanger design perspective. Among different approaches aimed at conductivity enhancement in storage systems with a phase change, application of metals or metal alloys directly as PCMs appears an intriguing concept. That is due to their much higher thermal conductivity when compared to "conventional" PCMs. This observation can be exemplified by a comparison of average thermal conductivity data for organic materials (from 0.15 up to 0.3 W/mK) or inorganic salt hydrates (from 0.4 up to 0.7 W/mK) with ther-

*e-mail: jkarwacki@imp.gda.pl

mal conductivity of selected low melting point metals or metal alloys (eg. from 8.1 up to even 86.9 W/mK) [10]. However, since no PCM could meet not only all, but even most of the expectations, the "advantages" and "disadvantages" of using metals or its alloys as PCMs need to be thoroughly analysed and weighed not to be overrated. Metallic PCMs are rather rarely addressed in literature when compared to organic and non-metallic inorganic phase changing materials. However, the idea of applying them as such is not a novelty, since probably the first ones to investigate the concept of LHS using metal PCM were Birchenall and Telkes already in 1976 [11]. Nevertheless, recently published articles [10, 12–14] indicate an emerging trend in the field of metal PCM-based heat storage in recent years. The thorough investigation of unique properties and application features of a "new" class of PCMs, being the *low* melting point liquid metals or their alloys, coupled with their comparison with "conventional" PCMs, was recently published in [10]. Still, literature dedicated to *middle* melting point PCMs[(1)] (40–200 °C, mostly Bi-based metal alloys), being of interest for authors of this paper, as well as *low* melting point metallic PCMs (0–30 °C, mostly Ga-based metal alloys) is very limited when compared to *high* melting point metallic PCMs (above 200 °C) [11, 15–19].

The general advantages of metallic PCMs, compared to non-metallic, "conventional" ones, apart from already mentioned (i) high thermal conductivity, are: (ii) high heat of fusion per unit volume, (iii) relatively low vapour pressure, (iv) moderate supercooling effect, (v) no phase separation, (v) non-flammability, (vi) long-term stability after millions of solidifying and melting processes. On the other hand, considering their disadvantages, mention may be made of: (i) significant weight, (ii) low heat of fusion per unit weight, (iv) low specific heat, (v) corrosion/stability/compatibility effect between metal and container as well as (vi) high cost of material [6, 10].

Blanco-Rodríguez et al. [12] analysed a performance of a magnesium and zinc eutectic alloy Mg51%-Zn (T_m = 342°C, ΔH_m = 155 J/g [13]) applied as a PCM and located in between two concentric tubes in a laboratory scale LHS unit. The results of systematic sets of experiments (heating and cooling tests) were used to validate a 2D model developed within Ansys Fluent CFD software. Application of the metal PCMs for TES system dedicated for direct steam generation concentrated solar power (DSG-CSP) was demonstrated and proved beneficial due to the quasi-constant melting and solidification temperatures and to its high heat transfer capacity. Nevertheless, Blanco-Rodríguez et al. [12] highlighted that even when high thermal conductivity PCMs was applied, the overall heat transfer was influenced by both conduction and convection phenomena and thus the latter also needed to be modelled. Kotze et al. [14] investigated application of a metallic PCM in the form of eutectic aluminium silicon AlSi12 (T_m = 577 °C, ΔH_m =462 J/g) for LHS in CSP both experimentally and mathematically. The test rig was constructed as a 1 m long cylinder, where AlSi12 was placed, with a heat transfer pipe running centrally through the container. Due to safety restrictions in the laboratory, it was not possible to apply liquid metals as metallic heat transfer fluids to heat the AlSi12 through the heat transfer pipe (this innovative approach was earlier suggested in [20]). Instead, the metal PCM was heated from the outside of a cylinder via electric heaters. Therefore only the discharge process was examined. The mathematical model was compared with the results of experiments during discharge process and confirmed the rationality of the concept. Still, the need for improving data accuracy with respect to material properties was noted.

2. Experimental set-up and procedure

The main objective of presented investigation is to create procedures for calculation and optimisation of shell-and-tube latent thermal energy storage unit with metals or metal alloys as PCMs. Therefore, the experimental study is focused on receiving the exact information about heat transfer between HTF and PCM during energy accumulation process. That is why simple geometry of heat transfer area was selected. Two configurations of shell-and-tube TES unit were investigated. Fig. 1. shows the scheme of the first shell-and-tube storage tank in which the length of heat transfer area is 2000 mm. The PCM was placed inside the inner tube and heat transfer fluid (HTF) flowed in a slot between the tubes. The PCM stored the thermal energy in both sensible and latent forms.

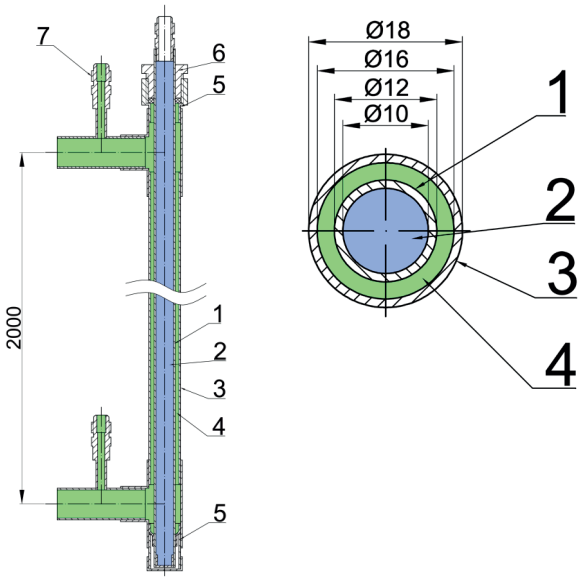

Fig. 1. Schematic view of shell-and-tube thermal energy storage (TES): 1 – inner tube, 2 – phase change material (PCM), 3 – outer tube, 4 – heat transfer fluid (HTF), 5 – leading ring, 6 – seal assembly, 7 – thermocouple mounting port

In the first LHS unit the inner diameter of outer tube is 16 mm and its wall thickness is 1 mm. The tube is covered throughout its length with 50 mm of mineral wool insulation and an aluminium cladding. There are two leading rings placed at the opposite tube sides to centre the inner tube. The slot between the inner and outer tubes is 2 mm. There is a seal as-

[(1)] Division into low, middle and high melting point metal PCM after [10]

sembly in the upper part of the tubes to allow a change of the internal tube. The inner diameter of internal tube is 10 mm and its wall thickness is 1 mm. Both tubes are made of copper. Construction of the second shell-and-tube storage tank is similar but the inner diameter of the tubes is 20 mm and 26 mm, respectively. Detailed information about both LHS units is listed in Table 1. Information in Table 1 is only relevant to the heat transfer part of LHS units (2000 mm).

Table 1
Primary information about the geometry of the two investigated LHS units.

		LHS 1	LHS 2
inner tube	inner diameter [mm]	10	20
	wall thickness [mm]	1	1
	weight [kg]	0.617	1.179
	volume of PCM [dm^3]	0.157	0.628
outer tube	inner diameter [mm]	16	26
	wall thickness [mm]	1	1
	weight [kg]	0.954	1.515
HTF	weight [kg]	0.183	0.314
PCM	weight [kg]	0.92162 kg	4.4560 kg

The LHS units were investigated on a test stand that was built in the Heat Transfer Department laboratory in IMP PAN. Fig. 2. shows the schematic view of the experimental set-up. The experimental system was composed of vertical shell-and-tube LHS unit, two Coriolis flow meters, two mixing valves, a pump, an electric circulation heater and a dry cooler. An ethylene glycol-water mixture was used as HTF. Two different

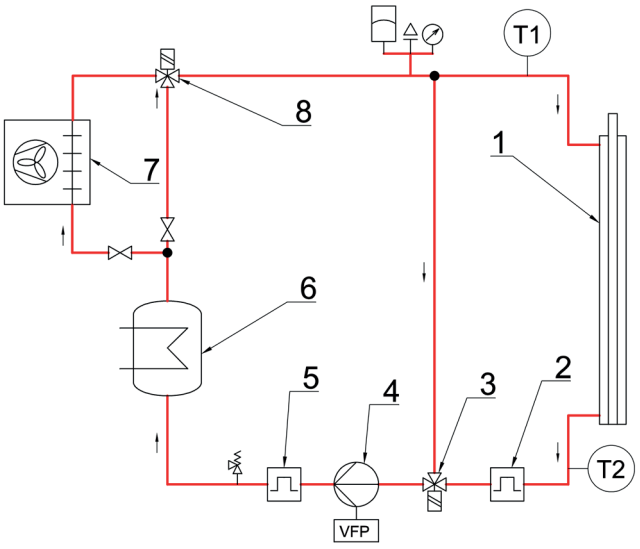

Fig. 2. Schematic diagram of the experimental set-up: 1 – LHS unit, 2 – Coriolis flow meter, 3 – control mixing valve, 4 – circulating pump, 5 – Coriolis flow meter, 6 – electric circulation heater, 7 – dry cooler, 8 – control mixing valve, T1 – inlet HTF temperature measurement, T2 – outlet HTF temperature measurement.

loops, separated by the 3-way control mixing valve (**3**), can be identified. The flow of the HTF was driven by the circulating pump (**4**). In the first loop an electric circulation heater (**6**) supplies HTF at a desired temperature. The power of electric heater **(6)** as well as the settings of circulation pump **(4)** and 3-way valves **(3,8)** are controlled by PI software regulators based on NI PXI platform and LabVIEW. The HTF flow rate in the second loop depends on position of the 3-way valve (**3**). In this manner suitable HTF temperature difference between the inlet and outlet of the LHS unit is achieved. The dry cooler (**7**) is used to cool HTF during the discharging process.

2.1. Description of metal alloy PCM

Sn60Bi40 was selected as a PCM for LHS unit under consideration in IMP PAN in Gdańsk [21]. With its melting temperature equal to 140.7°C, it falls into the category of *middle* melting point metal PCMs (40–200°C). The table below presents basic properties of the Sn60Bi40 and HTF fluid.

Table 2
Basic properties of the PCM and HTF used in experiments.

material	PCM	HTF
	Sn60Bi40	ethylene glycol-water mixture
density [kg/m^3]	8 545	1040
liquid phase specific heat [J/kgK]	2 130	3380
solid phase specific heat [J/kgK]	1 800	–
enthalpy of fusion [J/kg]	55 000	–
melting/solidification temperature [°C]	140.7	–
thermal conductivity [W/mK]	30	–

2.2 Test procedure

The results are evaluated on the basis of comparing inlet and outlet temperature, charging time and thermal energy stored by the LHS unit. The analysis involves constant temperature rise during charging test. This type of experimental procedure is similar to most common operating modes for differential scanning calorimetry (DSC) – a ramp temperature profile with constant heating rate. The charging experiments were initiated when the entire LHS unit with PCM and HTF was in steady state at about 100°C. In this state first reference value of heat losses was measured. Next, the charging process started. In this operating mode constant rate of inlet HTF temperature was hold at 0.01 K/s, 0.02 K/s, 0.03 K/s or 0.04 K/s, accordingly. The charging process was stopped when the inlet temperature reached about 152°C. Then, after reaching the steady state again, the second reference value of heat losses was measured. As shown in Fig. 2., the temperature evolution of HTF at the inlet and outlet of the test unit was monitored with two thermocouples **T1** and **T2** (of K-type). In order to achieve suitable

dynamic temperature response, 1 mm diameter thermocouples were used. The measurements of the PCM-filled storage units are compared to the reference results obtained with empty and water-filled inner tube.

3. Modelling of LHS unit thermal dynamics

Time variations of average temperatures in the investigated LHS unit were modelled with 0D model describing heat transfer between the HTF, PCM, the tubes' material and ambient air. The model equations are derived from the heat balances for each pair of the mentioned materials in contact, see Fig. 3. As the heat flow rate $\dot{Q}$ accumulated in the material of mass M and specific heat c depends on the difference between the inflow $\dot{Q}_{in}$ and outflow $\dot{Q}_{out}$ rates, these balances can be written in the following general form

$$\dot{Q} = Mc\frac{dt}{d\tau} = \sum \dot{Q}_{in}(\tau) - \sum \dot{Q}_{out}(\tau), \tag{1}$$

where t denotes temperature and τ is time. Adopting the designations given on the scheme in the Fig. 3, according to (1) balance equations for each of the heat accumulating material in the storage unit take forms presented below.

PCM:

$$M_P c_P(t)\frac{dt_P}{d\tau} = k_{PR}A_{PR}(t_R - t_P), \tag{2}$$

HTF:

$$\begin{aligned} M_H c_H \frac{dt_H}{d\tau} &= \dot{m}_H c_H (t_{Hi} - t_{He}) + \\ &+ k_{HR}A_{HR}(t_R - t_H) + k_{HZ}A_{HZ}(t_Z - t_H) \end{aligned}, \tag{3}$$

internal pipe R:

$$M_R c_R \frac{dt_R}{d\tau} = k_{PR}A_{PR}(t_P - t_R) + k_{HR}A_{HR}(t_H - t_R), \tag{4}$$

external pipe Z:

$$M_Z c_Z \frac{dt_Z}{d\tau} = k_{HZ}A_{HZ}(t_H - t_Z) - \dot{Q}_A. \tag{5}$$

In above equations, heat transfer from the liquid zones and surroundings was treated as purely convective. In the remaining zones, only conductive heat transfer was assumed. For the PCM zone, conduction occurs in the layer with the thickness of half of the internal radius of the pipe, $r_{Ri}/2$, as shown in Fig. 3. The balance for the HTF (3) was written in reference to average temperature t_H that is equal to arithmetic mean value of inlet and outlet temperatures,

$$t_H = \frac{t_{Hi} + t_{He}}{2}. \tag{6}$$

The heat capacity of the insulation U was omitted because of its low mass, therefore there is no balance equation for it. However, its influence on the heat transfer is included in the balance Eq. (5), in the heat flow rate $\dot{Q}_A$ lost to the ambient air A. The $\dot{Q}_{ZA}$ value was determined experimentally as a linear function of temperature difference $t_H - t_A$.

The overall heat transfer coefficient between the PCM and the internal pipe R is equal to

$$\frac{1}{k_{HR}} = \frac{\delta_R}{2\lambda_R} + \frac{1}{\alpha_R}, \tag{7}$$

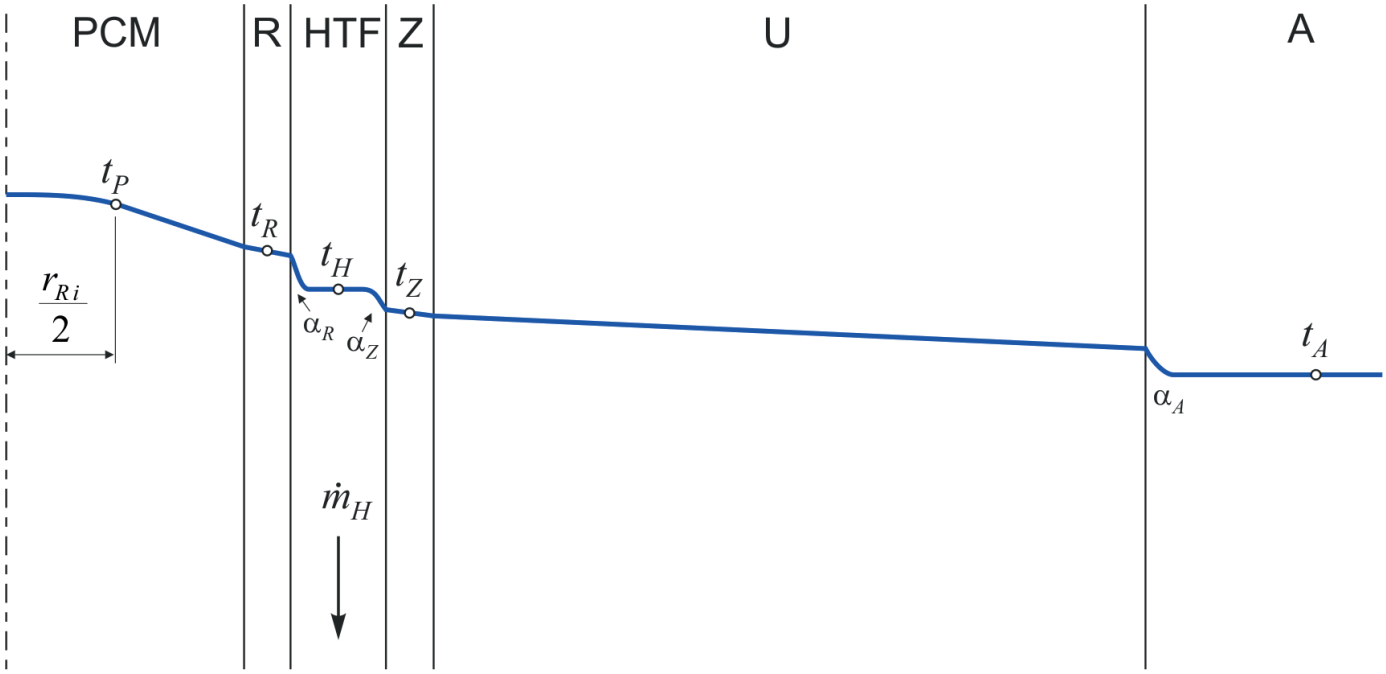

Fig. 3. Simplified temperature profile along the cross-section of the modelled heat storage unit assumed in derivation of 0D model equations

between the internal pipe R and the HTF:

$$\frac{1}{k_{HR}} = \frac{\delta_R}{2\lambda_R} + \frac{1}{\alpha_R}, \tag{8}$$

and between the HTF and the external pipe Z

$$\frac{1}{k_{HZ}} = \frac{\delta_Z}{2\lambda_Z} + \frac{1}{\alpha_Z}. \tag{9}$$

The HTF flow in the investigated storage unit was partially turbulent with the Reynolds number of about 5500 (for $\dot{m}_H = 200$ kg/h and $t_H = 140$°C). Therefore, the heat transfer coefficients α_Z and α_R in (8), (9) were determined from Hausen correlation corrected for the annular shape of the flow channel [22]. Their typical value was about 2300 W/m^{2}K. The values of overall coefficients k_{HZ} and k_{HR} were practically the same as α_Z and α_R, while the value of k_{PR} was considerably larger: 11800 W/m^{2}K.

PCM specific heat in the model is temperature dependent. It was assumed after [23] that its value is equal to the sum of single phase specific heat c_{mp} and two-phase specific heat c_{tp}, according to the following relationships:

$$c_P(t) = c_{mp}(t) + c_{tp}(t), \tag{10}$$

$$c_{mp}(t) = \frac{c_S + c_L}{2} + \frac{c_S - c_L}{2}\tanh(t - t_{SL}), \tag{11}$$

$$c_{tp}(t) = \frac{h_{SL}}{2}\left\{\tanh\left[B\left(t - t_{SL} + \frac{\Delta t_{SL}}{2}\right)\right] - \tanh\left[B\left(t - t_{SL} - \frac{\Delta t_{SL}}{2}\right)\right]\right\}, \tag{12}$$

where t_{SL} denotes the phase change temperature. According to [23], when the constant B in (12) is equal to 5, 90% of the phase change occurs in the temperature range of $t_{SL} \pm \Delta t_{SL}/2$. Exemplary specific heat distribution defined by equations (10)– (12) is presented in Fig. 4. Surface area under the curve c_P, in the phase change temperature range, is equal to the latent heat h_{SL}. Integration of equation (10) with respect to temperature results in enthalpy distribution (assuming c_P is the constant pressure specific heat). Exemplary result of such integration is depicted in Fig. 5, which shows that enthalpy is increased by the latent heat h_{SL} in the neighborhood of the phase change temperature t_{SL}.

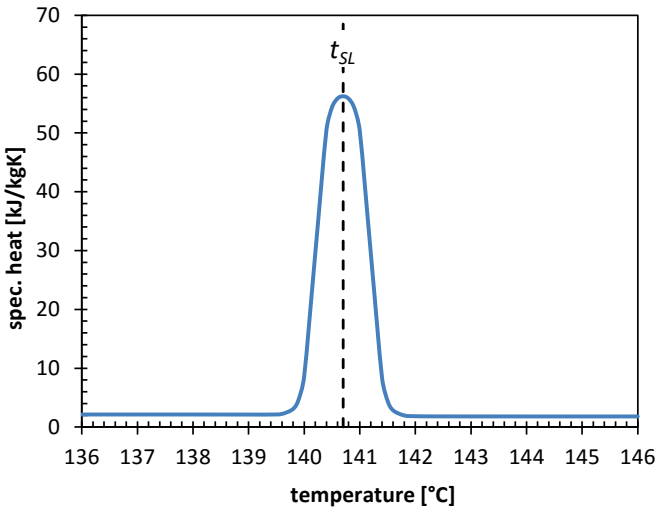

Fig. 4. Specific heat distribution of the PCM calculated from the equation (10) for Sn60Bi40 (comp. Table 2)

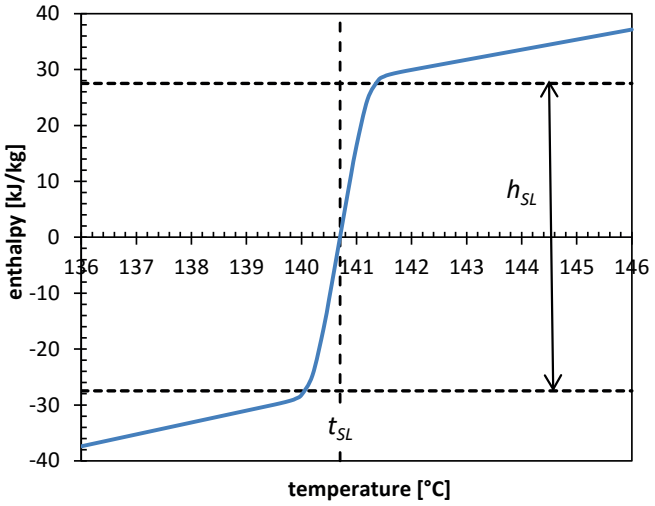

Fig. 5. PCM specific enthalpy distribution resulting from integration of the specific heat presented in Fig. 4. In the neighborhood of the phase change temperature t_{SL}, an increase of enthalpy by the latent heat occurs, marked with horizontal dashed lines

Solution of model equations (2)÷(5) for a predetermined inlet profile of HTF temperature t_{Hi} (τ) gives time distributions of average temperatures t_P (PCM), t_H (HTF), t_R (inner tube) and t_Z (outer tube). Next, from Eq. (6), outlet HTF temperature distribution can be calculated. Fig. 6 shows a difference between inlet (t_{Hi}, thermocouple T1) and outlet (t_{He} or T2) temperature calculated in this way with a constant heating rate dynamics.

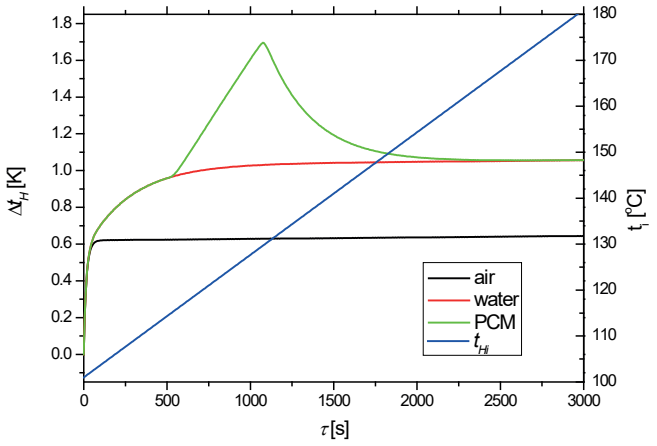

Fig. 6. Calculated difference between HTF inlet and outlet temperature Δt_H during a constant heating rate dynamics measurement as a function of charging process time: black line – empty tube, red line – water-filled tube, green line – tube with PCM. The profile of inlet HTF temperature tHi is also shown (blue line)

Table 3.
Results of the measurements performed for LHS 1 and LHS 2 units and used to determine heat losses ȮA.

run No.	LHS unit	$\dot{m}_H$ [kg/s]	Δt_{Hi} [K/s]	t_{Hi1} [°C]	t_{Hi2} [°C]	t_A [°C]	$\dot{Q}_{A1}$ [W]	$\dot{Q}_{A2}$ [W]
1	LHS 1	0.0556	0.0098	100.4	150.5	21.4	35.7	53.6
2	LHS 1	0.0555	0.0195	100.3	150.4	21.0	38.7	52.0
3	LHS 1	0.0555	0.0291	100.3	150.4	20.7	38.7	52.0
4	LHS 1	0.0556	0.0381	100.4	150.5	20.8	35.7	53.6
5	LHS 1	0.0832	0.0383	100.3	150.4	21.2	48.6	58.0
6	LHS 2	0.0555	0.0196	99.9	151.5	23.6	55.9	91.4
7	LHS 2	0.0555	0.0108	99.7	149.4	23.3	45.4	71.3

4. Results and discussion

Experimental studies were conducted in parallel with modelling aimed at elaboration of procedures for design and optimization of shell and tube storages with accumulation of heat in the latent form. Therefore, the results of experiments constitute an important element in verification of the proposed mathematical model as well as in determination of the necessary empirical coefficients. Heat storage units under investigation operate in dynamic systems and thus, the developed model includes time-dependent outlet temperature distributions depending on the inlet parameters. Due to the fact that the lumped parameters model does not take into account the geometry of the storage unit, validation based on the experimental results will enable verification of its suitability and, if necessary, introduction of correction factors.

First, reference tests were performed for empty and water-filled tanks and the heat accumulation in this case was of sensible type only. During these tests additional measurements were done to determine heat losses $\dot{Q}_A$ to the environment. For this purpose, the LHS units operated at constant inlet conditions with low (t_{Hi1} = 100°C) and high (t_{Hi2} = 150°C) HTF temperature and the obtained values of the heat flow rates $\dot{Q}_A$ are presented in Table 3. Fig. 7 and 8 exhibit the example results of experiments with the corresponding model prediction. Both figures show considerable fluctuations of the heat flux associated with the operation of the HTF heater. Divergence of experimental data and the values calculated theoretically originates from the transition period during the stabilization of the inlet temperature gradient. The obtained results indicate good agreement between the model and the experimental data.

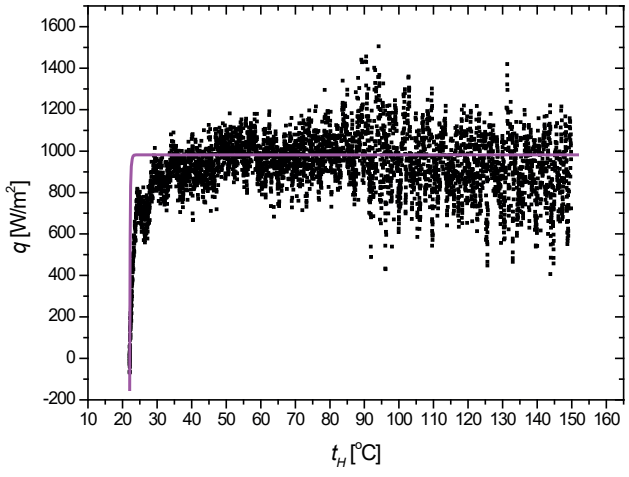

Fig. 7. The heat flux accumulated in the empty heat storage unit as a function of the average HTF temperature for the following experiment conditions: LHS 1, $\dot{m}_H$ = 200 kg/h, Δt_{Hi} = 0.03 K/s

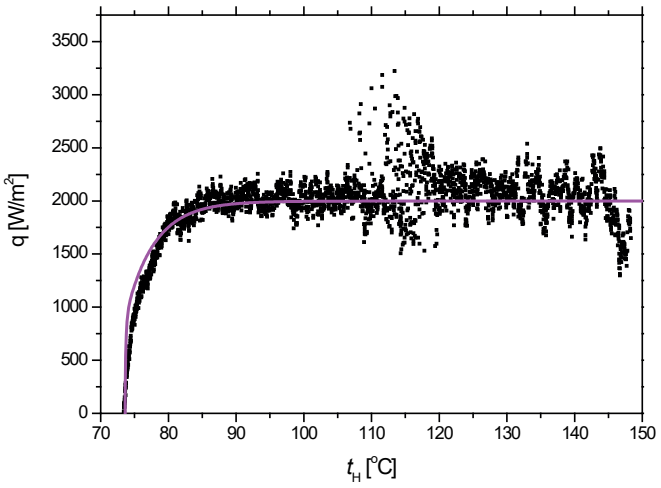

Fig. 8. The heat flux accumulated in the heat storage unit filled with water as a function of the average HTF temperature for the following experiment conditions: LHS 1, $\dot{m}_H$ = 200 kg/h, Δt_{Hi} = 0.03 K/s

The measurements conducted were dynamic in nature. They were done with a constant increase of temperature at the inlet of the heat storage unit (T_{Hi}). Execution of this kind of measurements requires a continuous change of the electric power of the liquid heater. In the case of small temperature difference between the inlet and outlet of the LHS unit, the implementation of such measurement with adequate precision is difficult. For the presented measurement results (Fig. 7 and 8) it is associated with significant fluctuations in the measured heat flux values.

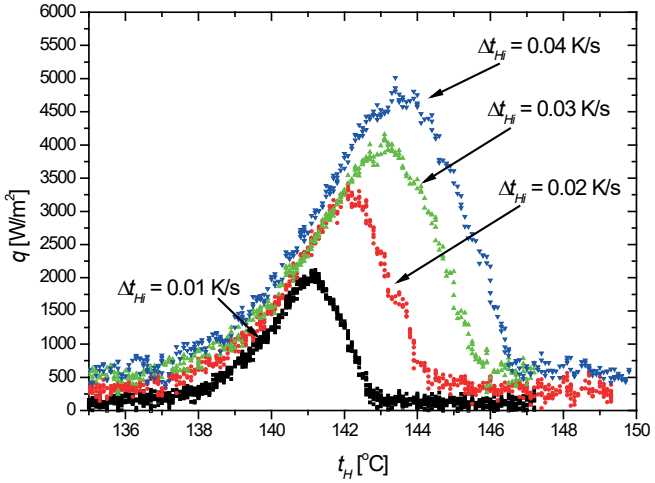

Fig. 9. The heat flux accumulated in the heat storage unit filled with Sn60Bi40 as a function of the average HTF temperature for the following experiment conditions: LHS 1, $\dot{m}_H$ = 200 kg/h

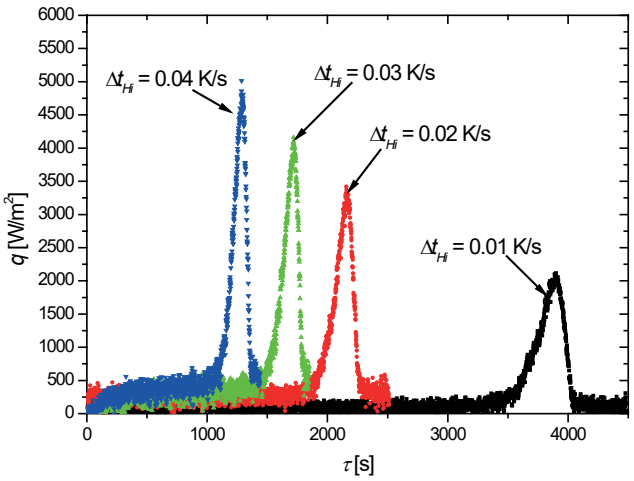

Fig. 11. Instantaneous values of heat flux accumulated in the storage unit as a function of time for selected gradients of average inlet temperature and the following experiment conditions: LES 1, $\dot{m}_H$ = 200 kg/h

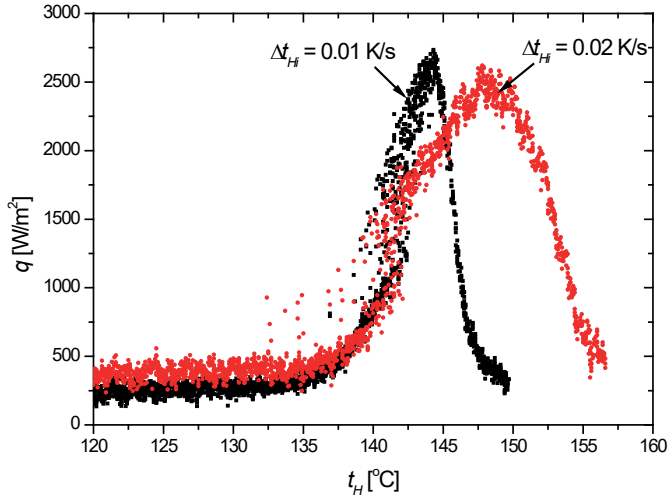

Fig. 10. Distribution of the heat flux accumulated in the latent heat storage unit as a function of the average HTF temperature for LHS 2 (after deduction of losses to the ambient environment).

Next, the measurements with PCM-filled storage units were performed and their results are presented in Fig. 9 and Fig. 10. A significant increase of heat flux accumulated in the storage unit within a temperature range corresponding to the phase transition in the eutectic alloy Sn60/Bi40 can be noticed. The shift of recorded temperature peaks towards higher temperatures is due to the dependence of temperature equalization in heat storage unit on the heating rate. For different heating rates, accumulated latent heat should be the same. In the presented measurements, a measure of this heat is the area under the curves presented in Fig. 11, which shows instantaneous values of accumulated heat flux during the experiment.

Due to dynamic nature of the measurements, detailed information on the conditions of heat transfer during its accumulation in the PCM requires a confrontation with the predictions of the presented mathematical model. A full analysis of the measurement results will be completed in the course of further work and will be published in a subsequent paper.

5. Conclusions

The main problem associated with the use of heat accumulators with phase changing materials is related to very low heat transfer on the PCM side, due to poor thermal conductivity. However, this is not the case for metallic materials and metal alloys. Nevertheless, proper design in the latter case also requires knowledge of the dependencies describing heat transfer process, particularly on the side of the PCM. The results of the charging process of a heat storage unit with eutectic SnBi alloy as PCM are presented in this paper. A test rig with a pipe in pipe LHS unit was described as well. The results of conducted experiments will be used for modification and verification of the developed mathematical model. Ultimately, the model will be used to design and optimise heat storage units with phase changing materials. Finally, the results show that the suggested metallic material may serve as a filling for a heat storage with short charging time and high heat capacity.

Acknowledgements. This project was supported by a grant from Polish National Centre for Research and Development.

References

[1] J. Chen, D. Yang, J. Jiang, A. Ma, and D. Song, "Research Progress of Phase Change Materials (PCMs) Embedded with Metal Foam (a Review)", *Procedia Materials Science* 4, 389–394, (2014).

[2] Z. Zhang, N. Zhang, J. Peng, X. Fang, X. Gao, and Y. Fang, "Preparation and thermal energy storage properties of paraffin/expanded graphite composite phase change material", *Applied Energy* 91, 426–431 (2012).

[3] L. Fan and J.M. Khodadadi, "Thermal conductivity enhancement of phase change materials for thermal energy storage: A review", *Renewable and Sustainable Energy Reviews* 15, 24–46 (2011).
[4] F. Agyenim, N. Hewitt, P. Eames, and Mervyn Smyth, "A review of materials, heat transfer and phase change problem formulation for latent heat thermal energy storage systems (LHTESS)", *Renewable and Sustainable Energy Reviews* 14, 615–628 (2010).
[5] S. Jegadheeswaran and S.D. Pohekar, "Performance enhancement in latent heat thermal storage system: a review", *Renewable and Sustainable Energy Reviews*, 13, 2225–2244 (2009).
[6] A. Sharma, V.V. Tyagi, C.R. Chen, and D. Buddhi, "Review on thermal energy storage with phase change materials and applications", *Renewable and Sustainable Energy Reviews* 13, 318–345 (2009).
[7] W. Wang, X. Yang, Y. Fang, J. Ding, and J. Yan, "Preparation and thermal properties of polyethylene glycol/expanded graphite blends for energy storage", *Applied Energy* 86, 1479–1483 (2009).
[8] J. Fukai, Y. Hamada, Y. Morozumi, and O. Miyatake, "Improvement of thermal characteristics of latent heat thermal energy storage units carbon-fiber brushes: experiments and modelling", *International Journal of Heat and Mass Transfer* 46, 4513–4525 (2003).
[9] A.D. Solomon, "Design criteria in PCM wall thermal storage", *Energy* 4 (4), 701–709 (1979).
[10] H. Ge, H. Li, S. Mei, and J. Liu, "Low melting point liquid metal as a new class of phase change material: An emerging frontier in energy area", *Renewable and Sustainable Energy Reviews* 21, 331–346 (2013).
[11] M.M. Kenisarin, "High-temperature phase change materials for thermal energy storage", *Renewable and Sustainable Energy Reviews* 14, 955–970 (2010).
[12] P. Blanco-Rodríguez, J. Rodríguez-Aseguinolaza, A. Gil, E. Risueño, B. D'Aguanno, I. Loroño, and L. Martín, "Experiments on a lab scale TES unit using eutectic metal alloy as PCM", *Energy Procedia* 69, 769–778 (2015).
[13] P. Blanco-Rodríguez, J. Rodríguez-Aseguinolaza, E. Risueno, and M. Tello, "Thermophysical characterization of Mg51%Zn eutectic metal alloy: A phase change material for thermal energy storage in direct steam generation applications", *Energy* 72, 414–420 (2014).
[14] J.P. Kotzé, T.W. von Backström, and P.J. Erens, "Simulation and testing of a latent heat thermal energy storage unit with metallic phase change material", *Energy Procedia* 49, 860–869 (2014).
[15] E. Risueño, A.Faik, J. Rodríguez-Aseguinolaza, P. Blanco-Rodríguez, A.Gil, M. Tello, and B. D'Aguanno, "Mg-Zn-Al eutectic alloys as phase change material for latent heat thermal energy storage", *Energy Procedia* 69, 1006–1013 (2015).
[16] M. Liu, W. Saman, and F. Bruno, "Review on storage materials and thermal performance enhancement techniques for high temperature phase change thermal storage systems", *Renewable and Sustainable Energy Reviews* 16, 2118–2132 (2012).
[17] T. Nomura, N. Okinaka, and T. Akiyama, "Technology of latent heat storage for high temperature application: a review", *ISIJ Int.* 50 (9), 1229–1239 (2010).
[18] J.Q. Sun, R.Y. Zhang, Z.P. Liu, and G.H. Lu, "Thermal reliability test of AL-34%Mg-6%Zn alloy as latent heat storage material and corrosion of metal with respect to thermal cycling", *Energy Conversion and Management* 48, 619–624 (2007).
[19] C.E. Birchenall and A.F. Riechman, "Heat Storage in Eutectic Alloys", *Metallurgical Transactions A*, 11A, 1415–1420 (1980).
[20] J.P. Kotzé, T.W. von Backstrom, and P.J. Erens, "High temperature thermal energy storage utilizing metallic phase change materials and metallic heat transfer fluids", *ASME: Journal of Solar Energy Engineering* 135, 1–6 (2013).
[21] K. Bogucka-Bykuć, W. Włosiński, and S. Bykuć, "Towards development of a prototype high-temperature latent heat storage unit as an element of a RES-based energy system (part 1)", *Bull. Pol. Ac.: Tech.* 62 (3), 489–494 (2014).
[22] H.D. Baehr, K. Stephan, *Heat and Mass Transfer*, 2nd Edition, Springer-Verlag, Berlin, 2006.
[23] P. Schalbart, D. Leducq, G. Alvarez, "Ice-cream storage energy efficiency with model predictive control of a refrigeration system coupled to a PCM tank", *Int. J. Refrigeration* 52, 140–150 (2015).